Anharmonicity Explains Temperature Renormalization Effects of the Band Gap in $SrTiO_3$

Yu-Ning Wu[1], Wissam A. Saidi[1,2], Jeffrey K. Wuenschell[1,3], Terumasa Tadano[4], Paul Ohodnicki[1], Benjamin Chorpening[1], Yuhua Duan[1*]*

[1]National Energy Technology Laboratory, United States Department of Energy, Pittsburgh, PA 15236, USA

[2]Department of Mechanical Engineering and Materials Science, University of Pittsburgh, Pittsburgh, PA 15261, USA

[3]Leidos Research Support Team, Pittsburgh, PA 15236, USA

[4]Research Center for Magnetic and Spintronic Materials, National Institute for Materials Science, Tsukuba, Ibaraki 305-0047, Japan

Email: yuhua.duan@netl.doe.gov; alsaidi@pitt.edu

Contents

Computational details for electron-phonon coupling

The ab initio DFT calculations were carried out using the projector augmented wave (PAW) method,[1] as implemented in the Vienna ab initio simulation package (VASP).[2-3] For the cubic primitive cell, a 12x12x12 Monkhorst-Pack k-point grid[4] is used. An energy cutoff of 550 eV and PBEsol exchange-correlation functional[5] are employed.

To include anharmonicity, the interatomic force constants up to the sixth order are extracted using a compressive sensing approach[6] from displacement-force datasets obtained by DFT calculations. The anharmonic phonon frequencies and polarization vectors are obtained using the self-consistent phonon (SCPH) method implemented in ALAMODE.[7-9] The harmonic and quartic force constants are processed using the SCPH theory, giving the renormalized phonons associated with the quartic anharmonicity. This method is able to provide not only the anharmonic phonon modes with the same quality as the temperature-dependent effective potential (TDEP) method at high temperature but also provide accurate phonon modes in low-temperature range due to the correct

treatment of the zero-point vibration.[8] A 2x2x2 supercell is used to obtain the force constants, and the SCPH is calculated at various temperatures by considering the quartic phonon-phonon interactions with 8x8x8 q-mesh, which is sufficiently dense to reach convergence.[8]

The electron-phonon coupling calculations are carried out using the finite displacement method as implemented in the nondiagonal supercell approach.[10-11] The shift of an eigenstate's energy level ϵ at temperature T is defined as

$$\Delta\epsilon(T) = \frac{1}{N_q}\sum_{\boldsymbol{q},\nu}\frac{a^{(2)}_{\boldsymbol{q}\nu;\boldsymbol{q}\nu}}{\omega_{\boldsymbol{q}\nu}}\left[\frac{1}{2} + n_B(\omega_{\boldsymbol{q}\nu}, T)\right], \quad \text{(S1)}$$

where $\boldsymbol{q}$ and ν are the phonon indices; N_q is the total number of the q points that sample the first Brillouin zone (FBZ); $a^{(2)}_{\boldsymbol{q}\nu;\boldsymbol{q}\nu}$ is the second-order electron-phonon coupling constant; $\omega_{\boldsymbol{q}\nu}$ stands for the phonon frequencies; n_B is the Bose-Einstein population of the phonons. In the framework of the finite-displacement method, the electron-phonon coupling constant is evaluated by examining the energy level shifts induced by the small atomic displacements following the eigenvectors of the phonon mode. $\Delta\epsilon(T = 0)$ is the zero-point (ZP) renormalization. Thermal lattice expansion also affects the electron structure, but it

is usually considered as a minor contribution.[12] Hence, the thermal expansion is neglected in this study.

Experimental method

To measure the temperature dependence of the optical band gap, 10 mm x 10 mm, 100-μm thick single crystal, two-side polished $SrTiO_3$ substrates (100) were purchased from MTI Corporation. One substrate was placed in a high-temperature Specac optical transmission cell with sapphire windows, with temperature measured via thermocouple in direct thermal contact with the sample holder. The optical transmission spectrum was measured from 300 to 950 K in 50-K increments. The optical transmission was measured by collimating a broadband balanced deuterium and halogen light source (Ocean Optics DH-BAL), transmitting it through the sample, and collecting the light to a fiber-coupled Ocean Optics Jaz spectrometer (190-890 nm). The baseline (100%) transmission was defined relative to an empty sample holder with windows in place.

To generate Tauc plots, the optical absorption coefficient was approximated as $\alpha(\lambda) = \left({}^{1}/_{d}\right)\ln\left({}^{100\%}/_{T(\lambda)}\right)$, based on the substrate thickness d and transmission

spectrum $T(\lambda)$. The Tauc method utilizes the approximately linear dependence of the plot $(\alpha(\varepsilon)\varepsilon)^{1/2}$ vs. photon energy $\varepsilon = hc/\lambda$; the y-intercept of a linear fit to this region is expected to approximately equal the optical band gap for an indirect semiconductor.[13]

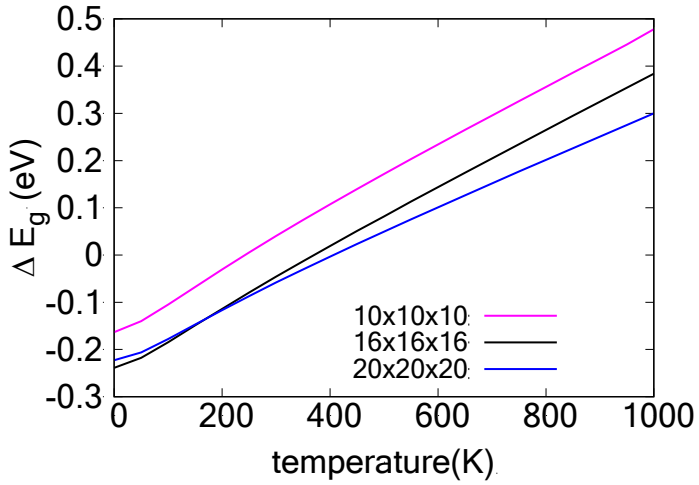

(a)

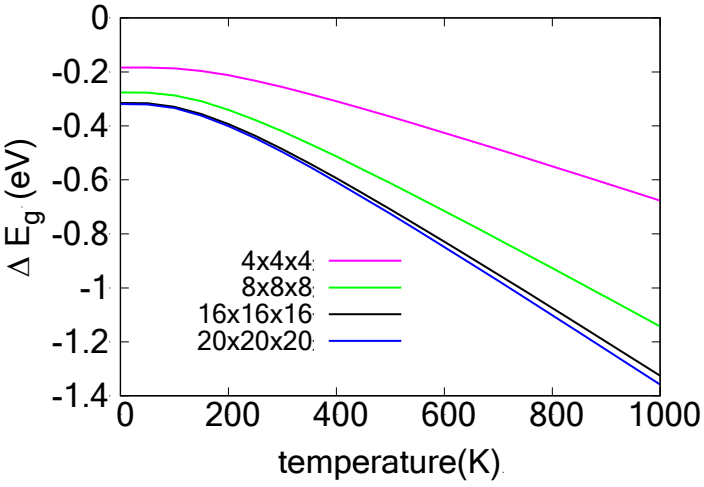

(b)

Figure S1. q-point mesh convergence tests for the calculation of band gap renormalization using (a) AHC theory with harmonic phonons and (b) FD approach with anharmonic phonons.

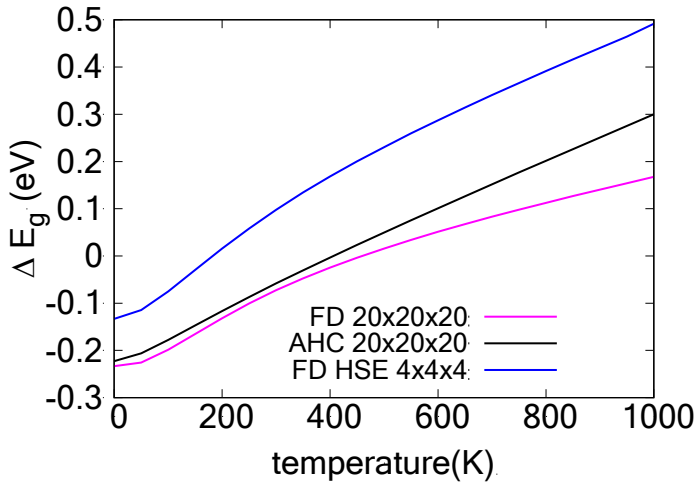

Figure S2. Comparison of band gap renormalization using PBEsol together with finite displacement method (magenta) and AHC theory (black), as well as a finite displacement calculation using HSE06 and 4x4x4 q-mesh (blue).

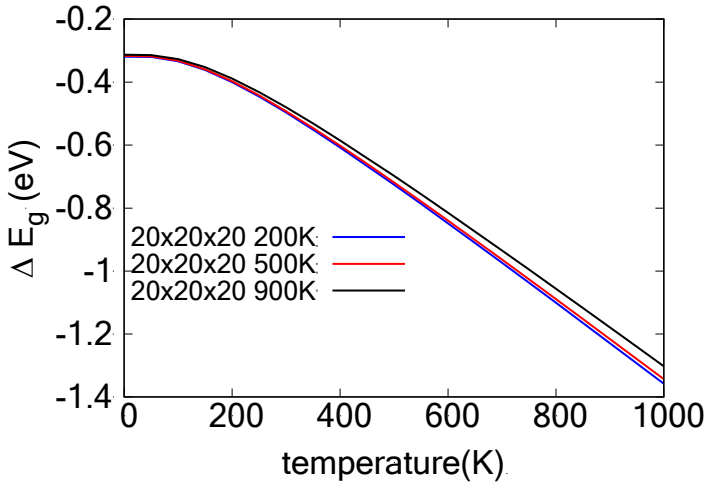

Figure S3. Band gap renormalization using the anharmonic phonon modes obtained at different temperatures.

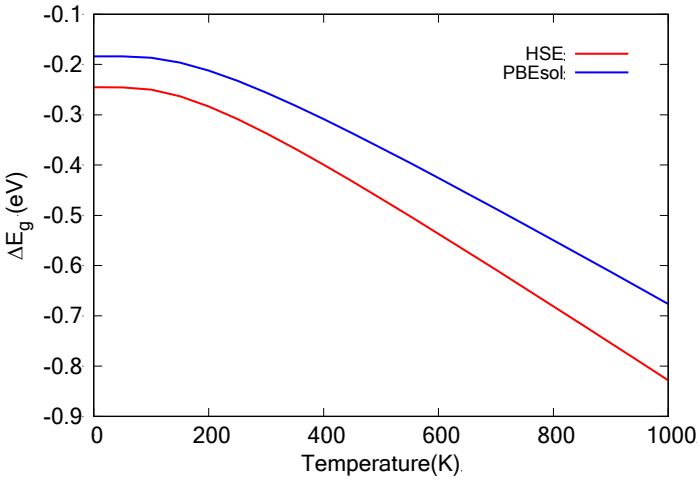

Figure S4: Comparison of band gap renormalization using PBEsol and HSE-06. 4x4x4 q-mesh is used for both curves.

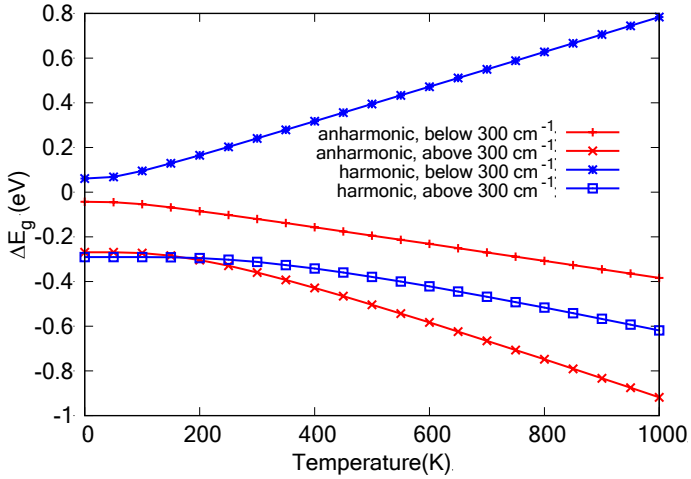

Figure S5: Comparison of the contributions from the modes above and below 300 cm^{-1} for calculations using harmonic and anharmonic phonon modes.

Computational methods and Results for optical properties

The frequency-dependent dielectric matrix in the long-wavelength limit and the optical properties can be calculated at the independent particle level.[14] The imaginary part of the dielectric constant tensor is calculated as

$$\varepsilon_2^{\alpha\beta}(\omega) = \frac{4\pi^2 e^2}{\Omega}\lim_{q\to 0}\frac{1}{q^2}\sum_{c,v,\boldsymbol{k}} 2w_{\boldsymbol{k}}\delta(\epsilon_{c\boldsymbol{k}} - \epsilon_{v\boldsymbol{k}} - \omega) \times \langle u_{c\boldsymbol{k}+\boldsymbol{e}_\alpha q}|u_{v\boldsymbol{k}}\rangle\langle u_{c\boldsymbol{k}+\boldsymbol{e}_\beta q}|u_{v\boldsymbol{k}}\rangle^*, \quad \text{(S2)}$$

where Ω is the volume of the primitive cell, $w_{\boldsymbol{k}}$ is the weight of each $\boldsymbol{k}$ point, and $\boldsymbol{q}$ is the wavevector. c and v are the conduction and valence band states, respectively. The $u_{c\boldsymbol{k}}$ is the periodic part of the Kohn-Sham orbital at the momentum $\boldsymbol{k}$. The $\boldsymbol{e}_\alpha$ and $\boldsymbol{e}_\beta$ are the unit vectors along three Cartesian directions. The real part of the dielectric tensor can be obtained from the imaginary part using Kramers-Kronig relations,

$$\varepsilon_1^{\alpha\beta}(\omega) = 1 + \frac{2}{\pi}P\int_0^\infty \frac{\varepsilon_2^{\alpha\beta}(\omega')\omega'}{\omega'^2 - \omega^2}d\omega', \quad \text{(S3)}$$

where P denotes the principal value. The optical conductivity σ, the index of refraction n and the extinction coefficient k are defined through[15]

$$\varepsilon(\omega) = \varepsilon_1(\omega) + i\varepsilon_2(\omega) = \frac{4\pi i}{\omega}\sigma(\omega) = (n + ik)^2. \quad \text{(S4)}$$

The optical properties at finite temperature are evaluated by a statistical average of the optical properties over a number of configurations that follow the lattice vibrations.[16] The configurations are generated as,

$$u_n = \sum_{\boldsymbol{q},\nu} u_{n,\boldsymbol{q}\nu} = \sqrt{\frac{1}{m_n}} \sum_{\boldsymbol{q},\nu} Q_{\boldsymbol{q}\nu} \hat{n}_{\boldsymbol{q}\nu} e^{i\boldsymbol{q}\cdot\boldsymbol{R}_n}, \quad \text{(S5)}$$

where u_n is the atomic displacement that is added to the atomic position of the ground state, m_n is atomic mass, $Q_{\boldsymbol{q}\nu}$ is the normal coordinate of the phonon branch ν at the momentum $\boldsymbol{q}$, and $\hat{n}_{\boldsymbol{q}\nu}$ is the eigenvector of phonons. In the second quantization representation, $Q_{\boldsymbol{q}\nu}$ can be written as

$$Q_{\boldsymbol{q}\nu} = \sqrt{\frac{\hbar}{\omega_{\boldsymbol{q}\nu}}} \left(b_{\boldsymbol{q}\nu} + b^{+}_{-\boldsymbol{q}\nu} \right),$$

where $b^{+}_{\boldsymbol{q}\nu}$ and $b_{\boldsymbol{q}\nu}$ are the creation and annihilation operators. We generate frozen-phonon configurations with $Q_{\boldsymbol{q}\nu}$ following the normal distribution function

$$P(Q_{\boldsymbol{q}\nu}) = \frac{1}{\sqrt{2\pi\sigma^2_{\boldsymbol{q}\nu}}} exp\left(-\frac{Q^2_{\boldsymbol{q}\nu}}{2\sigma^2_{\boldsymbol{q}\nu}} \right),$$

where $\sigma^2_{\boldsymbol{q}v} = \frac{\hbar}{2\omega_{\boldsymbol{q}v}}(2n_{\boldsymbol{q}v} + 1)$. The population $n_{\boldsymbol{q}v}$ is calculated from the Bose-Einstein distribution. The harmonic approximation is preserved in this fashion, because $\langle Q_{\boldsymbol{q}v} \rangle = 0$, and $\langle Q_{\boldsymbol{q}v} Q^*_{\boldsymbol{q}v} \rangle = \frac{\hbar(2n_{\boldsymbol{q}v} + 1)}{2\omega_{\boldsymbol{q}v}}$.

Following Equation (S5) and the anharmonic phonon modes obtained at temperatures 300 K, 700 K, 500K, and 1000 K, we employ a 3x3x3 k-point mesh for calculating the optical properties. The configurations are generated based on a 2x2x2 supercell, and DFT+U method with U=7eV is used for optical property calculation.[15] At each temperature, the $\varepsilon_1(\omega)$ and $\varepsilon_2(\omega)$ matrices are calculated by averaging over 50 configurations sampled from Equation (S5). Because of the cubic unit cell and its $Pm\bar{3}m$ symmetry, the diagonal element $\varepsilon^{xx}(\omega)$ is equal to $\varepsilon^{yy}(\omega)$ and $\varepsilon^{zz}(\omega)$. The values of the off-diagonal elements ($\varepsilon^{xy}(\omega)$, $\varepsilon^{yz}(\omega)$, $\varepsilon^{xz}(\omega)$) are very small and can be neglected. The results of $\varepsilon^{xx}(\omega)$ elements are shown in Figure. 5. Our results generally agree with previous experimental and theoretical studies.[15, 17-19] Figure S6(a) shows that the temperature has a smearing effect that smooths the $\varepsilon_1(\omega)$ and $\varepsilon_2(\omega)$ curves as high temperatures.

The refractive index n and extinction coefficient k can also be derived from the averaged $\varepsilon_1(\omega)$ and $\varepsilon_2(\omega)$, which are shown in Figure S6(b). Similar to the dielectric function, curves of *n* and *k* are smoother at higher temperatures. In the long-wavelength regime, the refractive index decreases as temperature increases from 0 K to 500 K, but increases from 500 K to 100 K (as shown in Figure S6(c)). Experimental results show that the refractive index decreases from the 50 °C and 400 °C (~323 K to 673 K), and the absolute value of the rate dn/dt decreases as well. This is consistent with our calculation between 0 K and 500 K.[20] The values of *n* in the long-wavelength limit (between 2.35 to 2.4) are also consistent with the experimental value 2.32.[21] Figures S6(d) shows the predicted optical conductivities of STO at selected temperatures. A similar smoothing effect is observed. The peaks get broadened as it approaches higher temperatures.

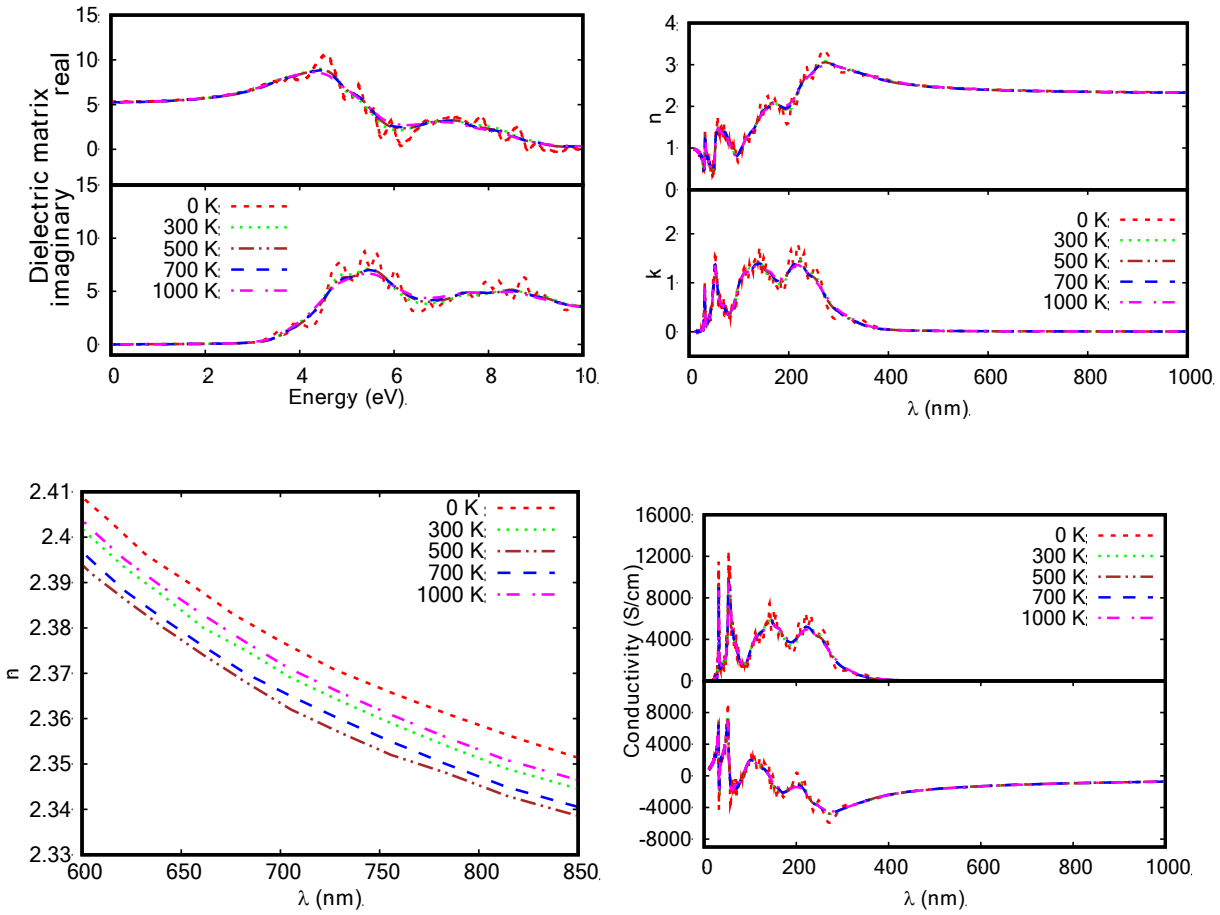

Figure S6. The calculated optical properties of STO. (a) The dielectric functions (ε_1^{xx}, ε_2^{xx}) at various temperatures. Real parts are shown in the upper panel, while imaginary parts are shown in the lower panel. (b) n and k at various temperatures. n is shown in the upper panel, while k is shown in the lower panel. (c) a zoomed view of (b) between 600 nm and 850 nm. (d) The optical conductivities at various temperatures. Real parts are shown in the upper panel, while imaginary parts are shown in the lower panel.

REFERNCE

(1) Blöchl, P. E. Projector Augmented-Wave Method. *Phys. Rev. B* **1994**, *50*, 17953.

(2) Kresse, G.; Furthmüller, J. Efficiency of *Ab-Initio* Total Energy Calculations for Metals and Semiconductors Using a Plane-Wave Basis Set. *Comput. Mater. Sci.* **1996**, *6*, 15-50.

(3) Kresse, G.; Hafner, J. *Ab Initio* Molecular Dynamics for Liquid Metals. *Phys. Rev. B* **1993**, *47*, 558.

(4) Monkhorst, H. J.; Pack, J. D. Special Points for Brillouin-Zone Integrations. *Phys. Rev. B* **1976**, *13*, 5188.

(5) Perdew, J. P.; Ruzsinszky, A.; Csonka, G. I.; Vydrov, O. A.; Scuseria, G. E.; Constantin, L. A.; Zhou, X.; Burke, K. Restoring the Density-Gradient Expansion for Exchange in Solids and Surfaces. *Phys. Rev. Lett.* **2008**, *100*, 136406.

(6) Nelson, L. J.; Hart, G. L.; Zhou, F.; Ozoliņš, V. Compressive Sensing as a Paradigm for Building Physics Models. *Phys. Rev. B* **2013**, *87*, 035125.

(7) Tadano, T.; Tsuneyuki, S. Self-Consistent Phonon Calculations of Lattice Dynamical Properties in Cubic $SrTiO_3$ with First-Principles Anharmonic Force Constants. *Phys. Rev. B* **2015**, *92*, 054301.

(8) Tadano, T.; Tsuneyuki, S. First-Principles Lattice Dynamics Method for Strongly Anharmonic Crystals. *J. Phys. Soc. Jpn.* **2018**, *87*, 041015.

(9) Tadano, T.; Gohda, Y.; Tsuneyuki, S. Anharmonic Force Constants Extracted from First-Principles Molecular Dynamics: Applications to Heat Transfer Simulations. *J. Phys.: Condens. Mat.* **2014**, *26*, 225402.

(10) Lloyd-Williams, J. H.; Monserrat, B. Lattice Dynamics and Electron-Phonon Coupling Calculations Using Nondiagonal Supercells. *Phys. Rev. B* **2015**, *92*, 184301.

(11) Monserrat, B. Electron–Phonon Coupling from Finite Differences. *J. Phys. Condens. Matter* **2018**, *30*, 083001.

(12) Wu, Y.-N.; Saidi, W. A.; Ohodnicki, P.; Chorpening, B.; Duan, Y. First-Principles Investigations of the Temperature Dependence of Electronic Structure and Optical Properties of Rutile TiO_2. *J. Phys. Chem. C* **2018**, *122*, 22642-22649.

(13) Stenzel, O. *The Physics of Thin Film Optical Spectra*; Springer, 2015.

(14) Gajdoš, M.; Hummer, K.; Kresse, G.; Furthmüller, J.; Bechstedt, F. Linear Optical Properties in the Projector-Augmented Wave Methodology. *Phys. Rev. B* **2006**, *73*, 045112.

(15) Duan, Y.; Ohodnicki, P.; Chorpening, B.; Hackett, G. Electronic Structural, Optical and Phonon Lattice Dynamical Properties of Pure-and La-Doped $SrTiO_3$: An *Ab Initio* Thermodynamics Study. *J. Solid State Chem.* **2017**, *256*, 239-251.

(16) Wu, Y.-N.; Zhang, X.; Pantelides, S. T. First-Principles Calculations Reveal Controlling Principles for Carrier Mobilities in Semiconductors. *Semicond. Sci. Technol.* **2016**, *31*, 115016.

(17) Marques, M.; Teles, L.; Anjos, V.; Scolfaro, L.; Leite, J.; Freire, V.; Farias, G.; da Silva Jr, E. Full-Relativistic Calculations of the $SrTiO_3$ Carrier Effective Masses and Complex Dielectric Function. *Appl. Phys. Lett.* **2003**, *82*, 3074-3076.

(18) Gogoi, P. K.; Schmidt, D. Temperature-Dependent Dielectric Function of Bulk $SrTiO_3$: Urbach Tail, Band Edges, and Excitonic Effects. *Phys. Rev. B* **2016**, *93*, 075204.

(19) Cardona, M. Optical Properties and Band Structure of $SrTiO_3$ and $BaTiO_3$. *Phys. Rev.* **1965**, *140*, A651.

(20) Toyoda, T.; Yabe, M. The Temperature Dependence of the Refractive Indices of $SrTiO_3$ and TiO_2. *J. Phys. D* **1983**, *16*, L251.

(21) Thomas, R.; Dube, D. Optical Properties of Sol–Gel Processed Amorphous and Crystalline $SrTiO_3$ Thin Films. *Jpn. J. Appl. Phys.* **2000**, *39*, 1771.